NJC

Accepted Manuscript

This article can be cited before page numbers have been issued, to do this please use: A. garcia-raso, A. Terron, A. Lopez-Zafra, A. García-Viada, A. Barta, A. Frontera, J. Loreznco, S. Rodriguez-Calado, E. M. Vazquez-Lopez and J. J. Fiol, *New J. Chem.*, 2019, DOI: 10.1039/C9NJ02279A.

This is an Accepted Manuscript, which has been through the Royal Society of Chemistry peer review process and has been accepted for publication.

Accepted Manuscripts are published online shortly after acceptance, before technical editing, formatting and proof reading. Using this free service, authors can make their results available to the community, in citable form, before we publish the edited article. We will replace this Accepted Manuscript with the edited and formatted Advance Article as soon as it is available.

You can find more information about Accepted Manuscripts in the author guidelines.

Please note that technical editing may introduce minor changes to the text and/or graphics, which may alter content. The journal's standard Terms & Conditions and the ethical guidelines, outlined in our author and reviewer resource centre, still apply. In no event shall the Royal Society of Chemistry be held responsible for any errors or omissions in this Accepted Manuscript or any consequences arising from the use of any information it contains.

View Article Online
DOI: 10.1039/C9NJ02279A

Journal Name

ARTICLE

Crystal structures of N^6-modified-aminoacid related nucleobase analogs (II): Hybrid Adenine-β-Alanine and Adenine-GABA molecules

Received 00th January 20xx,
Accepted 00th January 20xx

DOI: 10.1039/x0xx00000x

www.rsc.org/

Angel García-Raso[a], Angel Terrón[a], Adela López-Zafra,[a] Andrés García-Viada,[b] Agostina Barta,[a] Antonio Frontera[a,*], Julia Lorenzo[c], Sergi Rodríguez-Calado[c], Ezequiel M. Vázquez-López[d] and Juan J. Fiol[a,*]

In this manuscript we report the synthesis and X-ray characterization of four N^6-aminoacid/peptide-adenine-derivatives: N^6-βAlaAde·1.5H_2O (**1**) and N^6-GABAAde·2H_2O (**2**) and their corresponding protonated forms N^6-βAlaAde·HCl (**3**) and N^6-GABAAde·HCl (**4**). In (**1**) with neutral adenine ring, the protonated carboxylate interacts with the N(7) and N(6)H of the neighbour molecule. The hydrogen bond N9-H ···N(3) and the hydrogen bonds implying the water molecules are responsible of the planar and parallel disposition of the adenine rings. In (**2**), two different molecules are present in the crystal structure: a) A cationic unit in which the N(7)H tautomeric adenine is protonated at N(3) and the carboxylic group interacts with N(6B)-H and N(7B) of the adjacent molecule; b) An anionic unit, that presents the adenine ring in N(9)H tautomeric form, where the carboxylate interacts with the N(7A)H and N(6A)H of the neighbour adenine. In the hydrochloride form of N^6-βAlaAde (compound **3**) the aminoacidic chain with the carboxylic acid is almost orthogonal to the ring plane and exhibits protonation at N(3) of the adenine. On the other hand, in compound (**4**), the side chain is arranged parallel to the ring and anion(Cl^-)–π interactions are responsible of a parallel ordering of the final solid state architecture. We have studied the noncovalent interactions observed in the solid state architecture energetically using DFT calculations and rationalized the interactions using Molecular Electrostatic Potential surfaces and the Bader's theory of "Atoms-in-Molecules". The main purpose of this manuscript is to explore the competition between homodimer formation by the Hoogsteen site of the adeninium cation, self-association of the carboxylic group or through the interaction of the carboxylic group with the adeninium cation by X-ray crystallography.
.

1. Introduction

The purine skeleton exists in a wide variety of molecules either from natural[1] or synthetic sources.[2] Purine derivatives have a number of applications and are common targets in the synthesis of new therapeutic agents.[3] For instance, compounds containing the purine scaffold have been utilized as interferon inducers[4] and tested to treat chronic hepatitis C.[5] Moreover, they are used as cytostatic antitumor agents[6] and Hsp90 inhibitors. In particular, they induce the degradation of several Hsp90 client proteins associated to cancer.[7]

Adenine derivatives are promising therapeutic agents for the treatment of osteoporosis,[8] breast cancer,[9] inhibitors of cysteine protease cathepsin k[10] and as potent phosphodiesterase inhibitors.[11] Several N-substituted adenine derivatives have been reported as protein kinase inhibitors.[12] Furthermore, adenosine receptors participate in a variety of pathophysiological processes (inflammation and cancer).[13] In fact, diverse antagonists have been already reported in the literature.[14] The biological activity of all these adenine derivatives highly depends on the nature and position of the substituents on the heterocyclic ring. The capacity to synthesize new compounds, controlling their substitution pattern, is a relevant topic for research, diversifying the available adenine derivatives.

We and other have previously reported N^6-substituted adenines since they are interesting substrates due to their cytokinin activity.[15] Natural cytokinins (CK) are involved in most aspects of plant growth. They are modified adenine molecules with a side chain at the N^6-position that exhibit interesting biological properties including antiviral and antitumoral activities.[16] X-ray structural determination studies of N^6-modified-aminoacid/peptide nucleobase derivatives are scarce and very little structural information is available.[17] For instance, Krasnov *et al*. have described the synthesis, spectroscopic characterization and *in vitro* antimycobacterial activity of N-(2-aminopurin-6-yl) and N-(purin-6-yl) derivatives

[a.] Departament de Química, Universitat de les Illes Balears, Crta. de Valldemossa km 7.5, 07122 Palma (Baleares), Spain. E-mail: jfa950@uib.es; toni.frontera@uib.es
[b.] Facultad de Ciencias, Universidad Autónoma de Madrid
[c.] Instituto de Biotecnología y Biomedicina. Departamento de Bioquímica y Biologia Molecular. Universidad Autónoma de Barcelona. Barcelona. Spain.
[d.] Instituto de Investigación Sanitaria Galicia Sur/ Universidade de Vigo. Departamento de Química Inorgánica, Facultade de Química. Edificio Ciencias Experimentais. E-36310 Vigo. Galicia-Spain

*CCDC deposition numbers 1913605-1913608 contain the supplementary crystallographic data for compounds **1–4**.*

with amino acids and peptides.[17c] Recently, we reported the synthesis and X-ray crystal structures of N^6-aminoacid/peptide purines. [18] The packing of two hybrid adenine-glycine and glycylglycine molecules was described and revealed that H-bonding, anion-π and lp-π contacts were important in the packing of the solids. The supramolecular interactions of the nucleobases in biological systems are of great importance since they determine the folding and assembly of these systems.[19,20]

Herein, we report the synthesis, the lack of cytotoxicity[‡] and X-ray crystal structures of two N^6-aminoacid/peptide modified-adenine compounds, namely N^6-βAlaAde·1.5H_2O (**1**) and N^6-GABAAde·2H_2O (GABA = γ-aminobutyric acid) (**2**) and their corresponding protonated forms N^6-βAlaAde·HCl (**3**) and N^6-GABAAde·HCl (**4**) (see Scheme 1). We have analysed their X-ray solid state structure in detail. DFT calculations are used to evaluate the formation energy of several supramolecular assemblies, which are further characterized using the Bader's theory of "atoms-in-molecules".

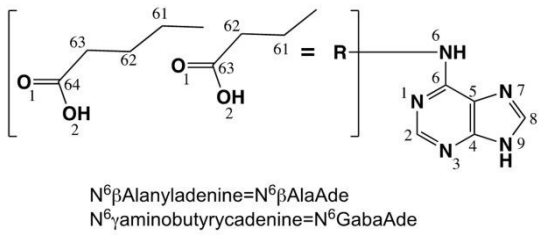

Scheme 1. Representation of the N^6-βAlaAde and N^6-GABAAde compounds and the atom-numbering scheme

2. Experimental

2.1. Materials and measurements

All chemicals were obtained from commercial sources (Sigma-Aldrich) and used without further purification. Elemental analyses of C, H and N were carried out on a Carlo-Erba (1106 and 1108) and Microanalyzer Thermo Finnigan Flash 1112 apparatus. FT-IR spectra in the solid state (KBr pellets) were measured in the 4000-400 cm^{-1} range on a Bruker Tensor 27 spectrometer. ^1H NMR spectra were recorded at room temperature on a Bruker AMX 300 (300MHz). Proton chemical shifts in DMSO-d_6 were referenced itself to DMSO-d_6 [^1H NMR δ= 2.50 ppm]. The N^6-βAlanine or GABA substituted adenines were obtained according to the previously described method by reaction of 6-chloropurine and β–alanine or γ-aminobutyric acid[17,21] and further detailed below.

2.2. Preparation of the compounds

Synthesis of N^6-βAlanyladenine·1.5H_2O (1).

A mixture of β–Alanine (10.6 mmol), 6-Chloropurine (5.3 mmol) and Na_2CO_3 (6 mmol) in 10 mL water were refluxed during 3.5 h. The resulting green solution was cooled and the pH adjusted to 3.5 using formic acid. An ochre-yellow-microcrystalline product was obtained, washed with water and air-dried (60% yield). Yellow monocrystals suitable for X-ray diffraction were collected from DMSO/MeOH 1:1 solution of the initial microcrystalline material. Anal. calcd for (**1**), $C_8H_{12}N_5O_{3.5}$ (234.21): C, 41.03; H, 5.16; N, 29.90. Found: C, 40.50; H, 5.12; N, 29.95. FT-IR (cm^{-1}): 1695m,sh, 1630s, 1604s, 1469m, 1413s, 1385m, 1311m, 1253w, 1229m, 1172w, 1034w, 963w, 906w, 793w, 675m, 636w, 537w. ^1H NMR, δ(300 MHz); DMSO-d6: 12.88s,br [N^+H], 8.19s [H8], 8.09s [H2], 7.55s,br [NH], 3.68s,br [HN-CH_2-], 2.58t, (J = 7.2 Hz)[CH_2-COO].

Synthesis of N^6-GABAadenine·2H_2O (2)

Yellow crystals of (**2**) were synthetized by the same method by using γ-aminobutyryc acid instead β-alanine. (60% yield). Anal. calcd for (**2**), $C_9H_{15}N_5O_4$ (257.1): C, 42.02; H, 5.88; N, 27.22. Found: C, 42.14; H, 5.85; N, 27.32. FT-IR (cm^{-1}): 3380s,br, 3286s, 1660s, 1628s, 1570sh, 1503m, 1468m, 1430m, 1402m, 1374m, 1321m, 1301m, 1244m, 1194m, 1139m, 977w, 781m, 706br,m, 629br,m, 543m. ^1H NMR, δ(300 MHz); DMSO-d6: 8.17s, 8.08s [H8,H2], 7.65s,br [NH], 3.49s,br [NH-CH_2-], 2.28t, (J = 7.2 Hz) [CH_2-COO], 1.83 quintuplet (J = 7.2 Hz) [-CH_2-].

Synthesis of N^6-βAlaAde·HCl (3) and N^6-GABAAde·HCl (4)

Light orange crystals of (**3**) and (**4**) were obtained by treatment of (**1**) and (**2**) respectively in HCl 2M. The obtained solution was refluxed during 2h. After two weeks of slow evaporation, suitable monocrystals were obtained in each case. Anal. calcd for (**3**), $C_8H_{10}ClN_5O_4$ (243.65): C, 39.44; H, 4.14; N, 28.74. Found: C, 39.45; H, 4.13; N, 29.15. FT-IR (cm^{-1}): 3121s,sh, 1739s, 1652s, 1608m, 1510m, 1483m, 1444s, 1424m, 1393w, 1356m, 1290s, 1214s, 779m, 615m, 632w. ^1H NMR, δ(300 MHz); DMSO-d6: 9.50s,br, 8.60s [H8], 8.51s [H2], 3.78s,br [NH-CH_2-], 2.68t (J = 6.9 Hz) [CH_2-COO]. Anal. calcd for (**4**), $C_9H_{12}ClN_5O_2$ (257.7): C, 41.95; H, 4.69; N, 27.18. Found: C, 41.68; H, 4.67; N, 27.05. FT-IR (cm^{-1}): 3121s,sh, 1739s, 1652s, 1608m, 1510m, 1483m, 1444s, 1424m, 1393w, 1356m, 1290s, 1214s, 779m, 615m, 632w. ^1H NMR, δ(300 MHz); DMSO-d6: 9.91s,br, 8.61s [H8], 8.57s [H2], 3.63d,br [NH-CH_2-], 2.38t (J = 7.2 Hz) [CH_2-COO], 1.88 quintuplet (J = 7.2 Hz) [-CH_2-].

2.3. Crystallographic analyses

A summary of the key crystallographic information is given in Table 1. Crystallographic data were collected at 100K on a Bruker D8 Venture diffractometer Photon 100 CMOS using an incoated high brilliance IμS microsource equipped with a Incoated HeliosTM multilayer optics. Data reduction and cell refinements were performed using the Bruker APEX3 program.[22a] Scaling and absorption corrections were carried out using the SADABS program in all cases. The structures were solved by direct methods using the program SHELXS.[22b] All non-hydrogen atoms were refined with anisotropic thermal parameters by full-matrix least-squares calculations on F^2 using the program SHELXL.[22b] Hydrogen atoms were generally inserted at calculated positions and refined as riders, except those of the –NH and –CO_2H groups and water molecule, which were generally located using a Fourier difference map and refined isotropically.

View Article Online
DOI: 10.1039/C9NJ02279A

Table 1. Crystal data and structure refinement parameters for **1** to **4**.

Empirical formula	$C_8H_{12}N_5O_{3.5}$ (**1**)	$C_9H_{15}N_5O_4$ (**2**)	$C_8H_{10}ClN_5O_2$ (**3**)	$C_9H_{12}ClN_5O_2$ (**4**)
Formula Weight	234.23	257.26	243.66	257.69
Wavelength (Å)	0.71073	0.71073	0.71073	0.71073
Crystal system	Monoclinic	Monoclinic	Monoclinic	Triclinic
Space group	*C 2/c*	*P 2₁/c*	*P 2₁/n*	*P-1*
a, b, c (Å)	a = 28.836(2)	a = 11.9730(14)	a = 4.4965(3)	a = 5.7390(3)
	b = 10.5330(8)	b = 12.7692(14)	b = 18.9802(13)	b = 9.8258(5)
	c = 7.2981(5)	c = 14.8340(18)	c = 11.8656(7)	c = 10.4109(5)
α, β, γ (°)	α=90	α=90	α=90	α=72.819(2)
	β=103.099(3)	β=95.582(4)	β=98.716(2)	β=85.079(2)
	γ=90	γ=90	γ=90	γ=85.218(2)
Volume (Å³)	2159.0(3)	2257.2(5)	998.74(11)	557.77(5)
Z/Density(calc.) (Mg/m³)	8/1.441	8/1.514	4/1.620	2/1.534
Absorption coeff (mm⁻¹)	0.115	0.121	0.376	0.341
F(000)	984	1088	504	268
Crystal size (mm³)	0.175 x 0.093 x 0.054	0.298 x 0.067 x 0.032	0.298 x 0.273 x 0.193	0.189 x 0.085 x 0.083
θ range for data collect	3.397 to 28.339°	2.629 to 28.401°	2.761 to 28.333°	2.174 to 28.318°
Limiting indices	-38≤h≤37, -14≤k≤14, -9≤l≤9	-15≤h≤16, -17≤k≤17, -19≤l≤15	-5≤h≤5, -25≤k≤25, -15≤l≤15	-7≤h≤7, -13≤k≤13, -13≤l≤13
Completeness to θ_{max} (%)	99.0 %	99.6%	99.7 %	99.9 %
Max. and min. transmission	0.7457 and 0.7228	0.7457 and 0.6798	0.7457 and 0.6685	0.7457 and 0.7178
Data/restraints/parameters	2672/3/179	5616/0/362	2458/0/157	2780/0/170
Goodness-of-fit on F²	1.081	1.023	1.116	1.090
Final R índices [I > 2σ(I)]	R1=0.086, wR2=0.1359	R1=0.0602, wR2=0.1350	R1=0.0307, wR2=0.0750	R1=0.0308, wR2=0.0708
R indices (all data)	R1=0.0855, wR2=0.1018	R1=0.1017, wR2=0.1551	R1=0.0334, wR2=0.0763	R1=0.0360, wR2=0.0732
Largest diff. peak and hole (e.Å³)	0.788 and -0.308	0.635 and -0.398	0.401 and -0.348	0.355 and -0.265
CCDC	1913605	1913606	1913607	1913608

2.4. Theoretical methods.

The calculations of the non-covalent interactions were carried out using the Gaussian-09[23] and the M06-2X/def2-TZVP level of theory.[24] To evaluate the interactions in the solid state, the crystallographic coordinates have been used. This procedure and level of theory have been successfully used to evaluate similar interactions.[25] The interaction energies have been computed by calculating the difference between the energies of isolated monomers and their assembly. The interaction energies were calculated with correction for the basis set superposition error (BSSE) by using the Boys–Bernardi counterpoise technique.[26] The Bader's "Atoms in molecules" theory (QTAIM) has been used to study the interactions discussed herein by means of the AIMall calculation package.[27] The molecular electrostatic potential surfaces have been computed using the Gaussian-09 software.[23]

3. Results and discussion

3.1. Description of the crystal structures of 1–4

Single crystal X-ray analysis revealed that (**1**), (**2**) and (**3**) crystallized in the monoclinic system with *C2/c*, *P2₁/c* and *P2₁*/n space groups respectively, while (**4**) is triclinic (*P-1*). A perspective view of N⁶-βAlaAde molecule (**1**), N⁶-GABAAde (**2**) and their protonated forms (**3**) and (**4**) are shown in Fig. 1. Selected hydrogen bonds are given in Table 2.

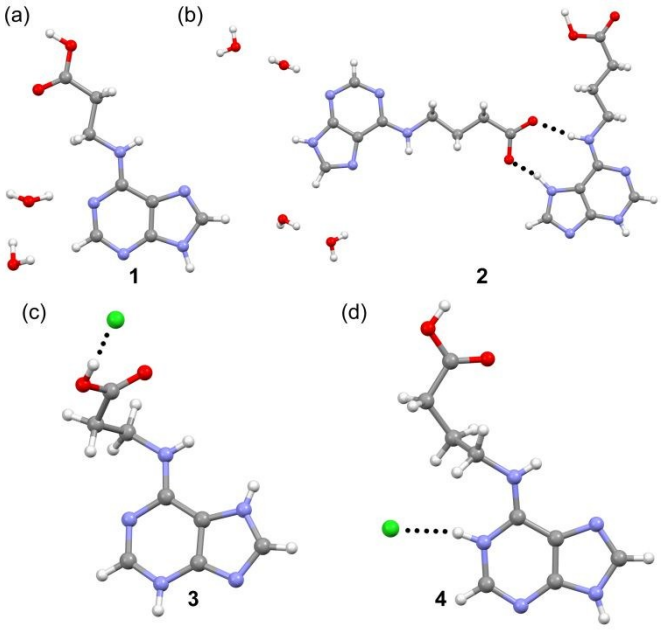

Fig. 1 X-ray structure of N⁶-βAlaAde·1.5H₂O (**1**), N⁶-AdeGaba·2H₂O (**2**), N⁶-βAlaAde·HCl (**3**) and N⁶-GABAAde·HCl (**4**).

View Article Online
DOI: 10.1039/C9NJ02370A

A comparison of the asymmetric unit of N^6-βAlaAde·1.5H_2O (**1**) with N^6-AdeGaba·2H_2O (**2**) shows interesting changes: while (**1**) is formed by neutral molecules with N(9)-H adenine tautomer, in (**2**) a pair of two different ionic molecules are present: the carboxylate anionic form of the N(9)-H adenine tautomer and protonated N(3) cationic form of the N(7)-H adenine tautomer. The tautomerism of carboxylate salts of adenine and pharmaceutically relevant N^6-substituted adenines have been analysed in detail[28] and the influence of hydrogen-bonding interactions and molecular recognition on tautomeric and protonation equilibria has been also studied, and some examples in which a non-canonical nucleobase tautomer is stabilized by a properly positioned H-bond acceptor have been reported in the literature.[29]

The crystal structure of (**1**) is dominated by a tandem of N(3)-H(3)···N(9) interactions between coplanar adenine rings that generate a self-assembled dimer (see Fig. 2a). Additional H-bonding interactions through the Hoogsteen face involving N(6)–H6 as donor and N(7) as acceptor and the COOH group of neighbour coplanar molecules complete the connectivity into the plane [O(1)–H···N(7) and O(2)···H6-N(6) H-bonds, see Fig 2a highlighted in pale green]. These 2D layers are connected by π-stacking interactions and reinforced by a network of hydrogen bonds thus generating the final 3D structure (see Fig. 2b).

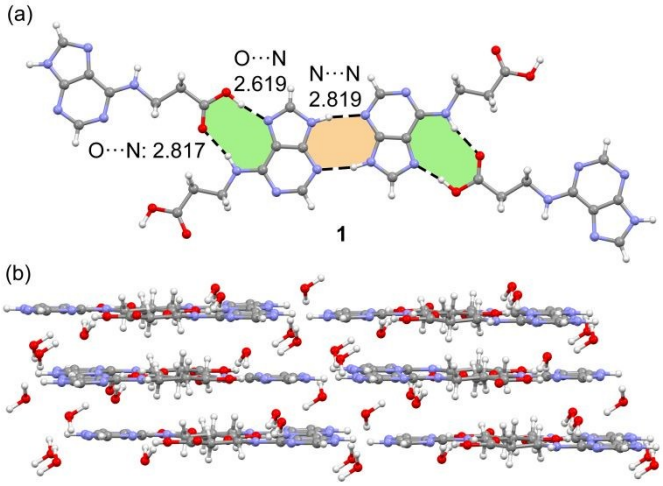

Fig. 2 X-ray solid state structure of compound (**1**). (a) Interactions into the plane (2D). Distances in Å (b) 3D crystal packing.

A characteristic fact of the asymmetric unit of (**2**) is the presence of two different ionic species (organic salt). That is, the cationic A unit with the N(3) and COOH protonated and the anionic B form with neutral ring and deprotonated carboxylate group. A representation of the 2D interactions is shown is Fig. 3 as well as the final 3D packing. The 2D layer represented in Fig 3a is stabilized by a network of H-bonding interactions. Curiously the protonated N(3)–H group does not participates in this network because it is blocked by a water molecule. In addition to the N(7)–H···N(9) adenine···adenine H-bond that connects the counter-ions through the five membered rings, the hydrogen bonding network is generated by the formation of O–H···N and N–H···O contacts (see Table 2 for the H-bonding geometric features) between the Hoogsteen face of adenine and the carboxylic/carboxylate groups of the side chains. In case of the anion (B), N7 acts as H-bond acceptor (see green coloured supramolecular ring in Fig.3a) and the carboxylic group is protonated. On the contrary, for the cation (A), the N7–H group acts as H-bond donor (see buff coloured supramolecular ring) and the carboxylic group is deprotonated. The final 3D architecture is generated by the stacking of these 2D layers as detailed in Fig. 2b.

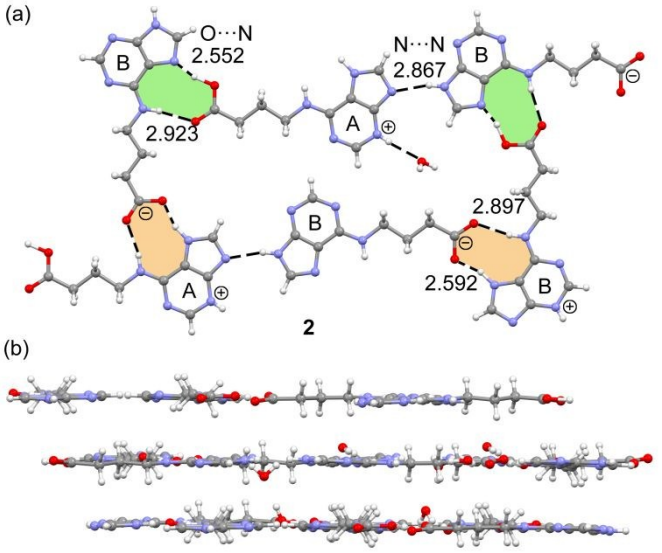

Fig. 3 (a) 2D layer formed in compound (**2**) by means of H-bonding interactions. (b) final 3D architecture.

Previous works have used adenines substituted with –$(CH_2)_n$–COOH groups as minimalistic model systems to interpret protein-nucleic acid interaction. Specifically, the presence of a carboxyl group in adenine derivatives has been studied to mimic adenine-aspartic/glutamic acid interaction.[30] In addition, it has been demonstrated that the hydrogen bonding pattern of adeninium cation having incorporated –$(CH_2)_2$–COOH at N9 position depends on the counterion. For instance, the nitrate and chloride promote self-dimerization of adeninium cation moiety through the Hoogsteen face. In contrast, the trifuoroacetate induces the cross-dimerization between carboxylic group and the Hoogsteen face of adeninium cation.[30b]

We have obtained the hydrochloride salts of compounds (**1**) and (**2**) to analyze the competition between homodimerization of the adeninium cation through the Hoogsteen site, cross-dimerization where the carboxyl group interacts with the Hoogsteen face of the adeninium cation and finally, homodimerization of the carboxyl group.

Unexpectedly, compound (**3**) exhibits the N(3) atom of adenine protonated instead of the more common N(1) protonation site, see Fig. 1c. Moreover, the tautomeric form of (**3**) is N(7)–H and, consequently, these cations occur as dimers in the solid state crystal structure, hydrogen bonded across a centre of symmetry, with an N(3)–H···N(9) distance of

View Article Online
DOI: 10.1039/C8NJ02270A

2.812(3) Å. It is possible that the occurrence of these dimers leads to the N(3) protonation instead of N(1). It is also worth mentioning that the Hoogsteen site of adeninium is blocked by a chloride anion that establishes a bifurcated H-bond with N(6)–H and N(7)–H groups. The H-bonded dimers stack in zig-zag columns along the c axis, with partial π···π stacking between the imidazole and the six membered rings, as represented in Fig. 4b.

Table 2. Selected hydrogen bonds [d(D-H) ≤ 1.02 Å and <(DHA) > 150°] for (**1**) to (**4**) [Å and °]. See Scheme 1 for atom numbering.

(1)

D-H···A	d(D-H)	d(H···A)	d(D···A)	<(DHA)
O(1)-H(1)···N(7)#1	0.99(3)	1.64(3)	2.6185(17)	170(2)
N(6)-H(6)···O(2)#2	0.88(2)	1.95(2)	2.8173(17)	167.6(19)
N(9)-H(9)···N(3)#4	0.93(3)	1.90(3)	2.8189(17)	167(3)
O(1W)-H(1W2)···O(1) #1	0.99(3)	1.96(3)	2.8855(18)	155(2)
O(2W)-H(2W2)···O(1W)	1.02(4)	1.85(6)	2.782(4)	151(6)

#1 –x+½,y-½,-z+½; #2 -x+½,y+½,-z+½; #4 –x,-y+2,-z+1

(2)

D-H···A	d(D-H)	d(H···A)	d(D···A)	<(DHA)
C(32)-H(32)···O(1W)	0.95	2.36	3.283(3)	163.0
C(2A)-H(2A)···N(1B)#1	0.95	2.57	3.400(3)	146.2
N(3A)-H(3A)···O(1W)#2	0.73(3)	2.02(3)	2.727(3)	164(3)
N(6A)-H(6A)···O(1B)	0.88	2.03	2.897(2)	168.8
N(7A)-H(7A)···O(2B)	1.02(3)	1.58(3)	2.572(2)	163(2)
C(8A)-H(8A)···O(3W) #2	0.95	2.63	3.508(3)	154.5
N(6B)-H(6B)···O(2A)#4	0.88	2.05(4)	2.923(2)	170.9
N(9B)-H(9B)···N(9A)#5	0.84(3)	2.05(3)	2.867(3)	165(2)
O(1W)-H(1W1)···O(3W)#6	0.77(4)	1.92(4)	2.660(3)	161(4)
O(1W)-H(1W2)···O(2W)	0.83(4)	1.94(4)	2.756(3)	172(3)
O(3W)-H(3W1)···O(4W)	0.82(4)	1.94(4)	2.709(3)	155(4)
O(4W)-H(4W1)···O(2B)#5	0.81(3)	1.96(3)	2.750(2)	164(3)
O(4W)-H(4W2)···O(2A)#3	0.86(3)	1.93(3)	2.794(2)	177(3)
O(2W)-H(2W1)···O(1B)#4	0.80(3)	1.96(3)	2.755(2)	175(3)
O(2W)-H(2W2)···O(1A)#4	0.79(3)	2.07(3)	2.857(2)	170(3)
O(1A)-H(1A)···N7B#7	1.19(2)	1.38(2)	2.552(2)	165(2)

#1 x+1,-y-½,z+½; #2 x+1,-y-3/2,z+½; #3 x-1,-y-½,z-½; #4 x,y-1,z;
#5 x-1,-y-3/2,z-½; #6 -x+1,y-½,-z-½; #7 x, 1+y, z

(3)

D-H···A	d(D-H)	d(H···A)	d(D···A)	<(DHA)
N(6)-H(6)···Cl(1)#5	0.843(17)	2.426(18)	3.2626(12)	171.9(15)
O(2)-H(10)···Cl(1)	0.858(18)	2.168(18)	3.0199(12)	172.1(15)
N(3)-H(3)···N(9)#6	0.874(17)	1.973(17)	2.8125(15)	160.4(15)
N(7)-H(7)···Cl(1)#6	0.795(18)	2.432(18)	3.1826(11)	157.9(15)

#5 x+½,-y+½,z+½; #6 -x+1,-y-½,-z+2

(4)

D-H···A	d(D-H)	d(H···A)	d(D···A)	<(DHA)
O(1)-H(1)···N(7)#4	0.90(2)	1.83(2)	2.7290(15)	170(2)
N(6)-H(5)···O(2) #4	0.821(18)	1.970(18)	2.7734(14)	165.7(17)
N(9)-H(3)···N(3)#5	0.847(19)	2.112(19)	2.9295(15)	162.2(18)
N(1)-H(4)···Cl(1)	0.88(2)	2.18(2)	3.0306(11)	162.3(17)

#4 -x-1,-y,-z; #5 –x+1, -y+1, -z-1

In case of hydrochloride (**4**) the expected N(1) is the protonation site in the adenine ring and the tautomer is N(9)-H (Fig 1c). Similarly to compound (**3**), it forms adenine homodimers in the solid state via two symmetrically equivalent N(9)–H···N3 H-bonds (highlighted in green, see Fig. 5a). Moreover, additional self-assembled dimers are formed via two sets of [O(1)-H(1)···N(7) and N(6)-H(5)···O(2)] hydrogen bonds (highlighted in buff colour, see Fig. 5a) Both types of supramolecular assemblies generate the formation of infinite 1D tapes. These tapes stack generating 2D supramolecular sheets (see Fig 5b) with partial π···π stacking between five membered rings (see Fig 5c). The chloride anions, in addition to the formation of several H-bonds connecting the adenine moieties, they establish Cl···π interactions, as indicated in Fig. 5c. The interaction is basically with the protonated N(1) atom of the adeninium moiety (3.239 Å).

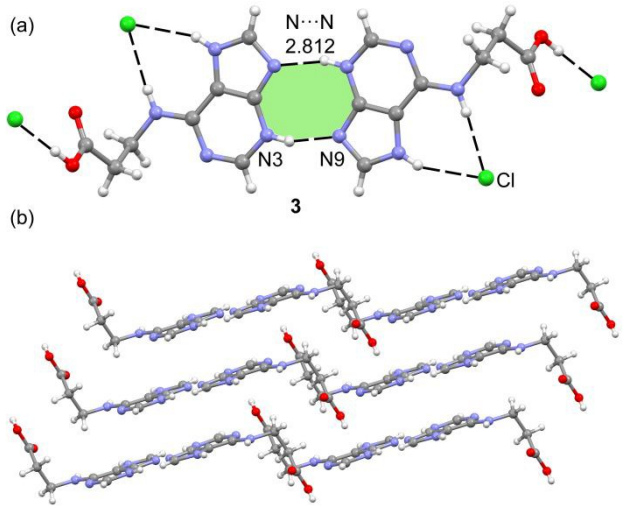

Fig. 4 (a) Detail of dimers in compound (**3**). (b) zig zag columns generated through π-π stacking interactions.

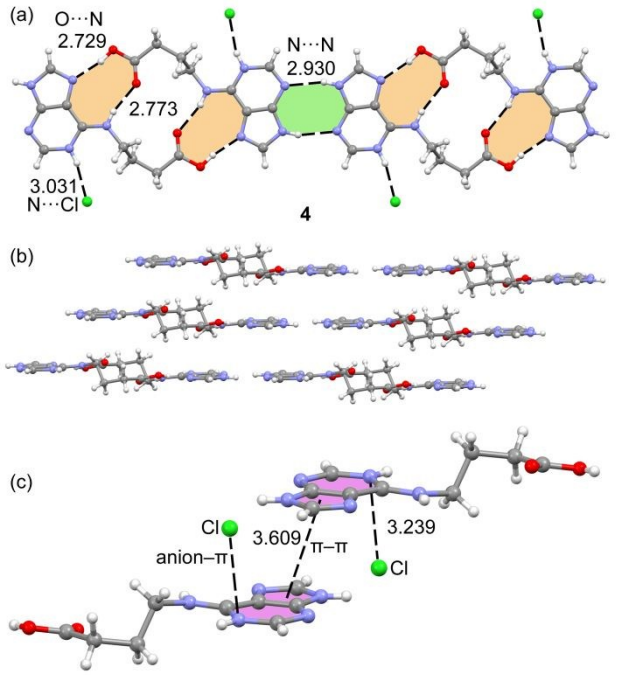

Fig. 5 (a) Detail of dimers in compound (**4**). (b) packing of dimer units through π-π stacking interactions. (c) Detail of the anion–π/π–π/anion–π assembly

3.2 Theoretical Study

To gain an insight into the different modes of interaction described above, we have performed a DFT at the M06-

View Article Online
DOI: 10.1039/C9NJ02270A

2x/def2-TZVP level of theory. The hydrogen bond energies were determined using two methodologies. First, we have used the common equation $\Delta E = E_{(A\cdots B)} - (E_A + E_B)$ [Eq. 1] where $E_{(A\cdots B)}$ is the energy (kcal/mol) of the H-bonded dimer and E_A and E_B depict the energy of the individual monomers. Secondly, we have used the QTAIM and the value of the kinetic $G(r_{CP})$ contributions to the local energy density of electrons at the critical point (CP). We have computed the energies for each individual H-bonding contacts according to the conventional approach by Vener *et al.*[31] that was specifically developed for HBs [Energy = 0.429 * G(r) at the bond CP]. The latter method is convenient to know the individual contribution of each contact and also to evaluate the influence of the H-bonding in the presence of other interactions.

In Fig. 6a we show the molecular electrostatic potential plotted onto the van der Waals surface for compound (**1**) as a model of N^6-carboxyalkyl substituted adenine. The MEP surface analysis is adequate to know the electron rich and electron poor regions of the molecule. It can be observed that the most positive region corresponds to the carboxylic acid (+56 kcal/mol) followed by N9–H (+50 kcal/mol) and finally N6–H (+36 kcal/mol). Moreover, the most negative parts correspond to the N1 (–35 kcal/mol), followed by the O-atom of the COOH group (–34 kcal/mol) and the N3 atom (–33 kcal/mol). The MEP is also negative at the N7 atom (–29 kcal/mol).

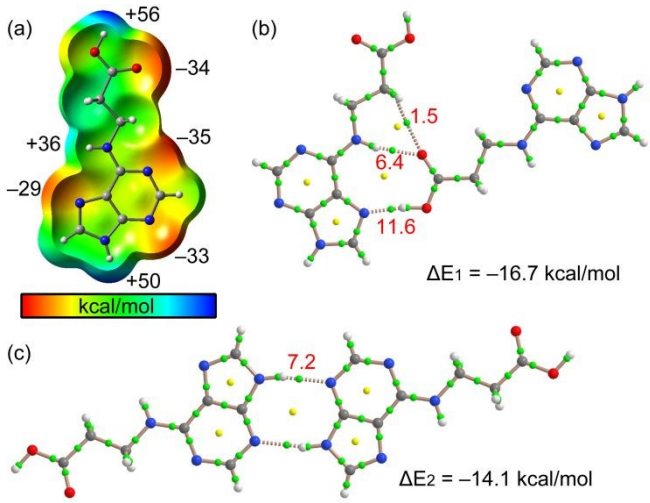

Fig. 6 (a) MEP surface of compound (**1**) at the M06-2X-def2-TZVP level of theory. Isosurface 0.001 a.u. The energies at selected points of the surface are indicated. (b,c) AIM distribution of bond and ring critical points (green and yellow spheres, respectively) and bond paths obtained for two dimers of compound (**1**). The interaction energies are indicated. The dissociation energy of the H-bond using the G(r) values at the bond CP are indicated in red (kcal/mol).

In Fig. 6 we have also represented the distribution of bond critical points (CP) and bond paths for the two dimers that are responsible for the formation of the 2D layer in compound (**1**), as aforementioned in Fig. 2a. The QTAIM analysis shows the presence of appropriate bond CPs (3, –1) and bond path between the N/O and H atoms for the intermolecular H-bonds interactions in both dimers. Moreover, ring CPs (yellow spheres) also emerge upon complexation due to the formation of supramolecular rings. For the dimer shown in Fig. 6b, the distribution also shows the existence of a weak C–H···O interaction between the H-atom of the alkyl chain and the O atom of the carboxylic group. The interaction energy of this dimer is ΔE_1 = –16.7 kcal/mol, which is larger in absolute value than that obtained for the self–assembled dimer (see Fig. 6c, ΔE_2 = –14.1 kcal/mol). We have also indicated in Fig. 6 the individual energy of each H-bond, which was estimated using the QTAIM method by means of the kinetic energy G(r) values at the bond CPs. For the self-assembled homodimer (see Fig. 6c), the agreement between the interaction energy computed using Eq. 1 (–14.1 kcal/mol) or the QTAIM (–14.4 kcal/mol) is excellent. For the dimer where the carboxylic group interacts through the Hoogsteen face of adenine, the interaction energy using the QTAIM is slightly overestimated (–19.5 kcal/mol). The strongest H-bonds corresponds to the O–H···N(7) in agreement with the shortest O···N distance observed experimentally and the acidity of the H-bond donor.

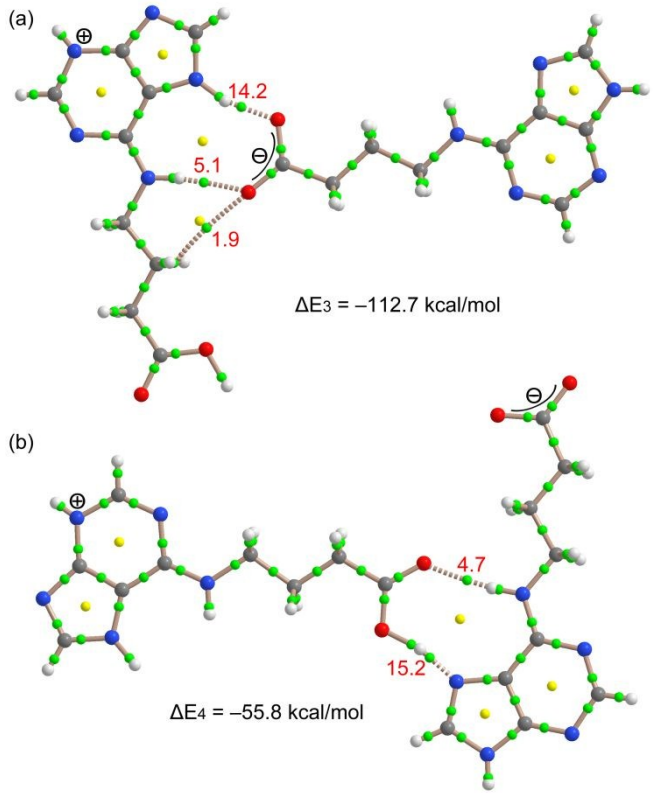

Fig. 7 (a,b) AIM distribution of bond and ring critical points (green and yellow spheres, respectively) and bond paths obtained for two dimers of compound (**2**). The interaction energies are indicated. The dissociation energy of the H-bond using the G(r) values at the bond CP are indicated in red (kcal/mol).

For compound (**2**) (organic salt) we have studied the energetic features of both dimers that govern the formation of the 2D supramolecular sheet represented in Fig. 3a. The interaction energies are very large due to the electrostatic attraction of both counterions. In fact, the dimer represented in Fig 7a exhibits a very large binding energy ΔE_3 = –112.7 kcal/mol, much larger than the dimer of Fig. 7b (ΔE_4 = –55.8 kcal/mol)

simply because the separation of the opposite charges is smaller. In this case, it is very useful to use the individual energies obtained from the QTAIM analysis, because they are free from purely electrostatic effects. Interestingly, for the interaction where the carboxylate interacts with the adenine (Fig. 7a), the QTAIM analysis shows the existence of an ancillary C–H···O interaction in addition to the expected N–H···O H-bonds, similarly to that described above for compound (**1**) (see Fig. 6a). This interaction is the weakest one (–1.9 kcal/mol), and the sum of the three interactions (–20.9 kcal/mol) is comparable to the interaction estimated for compound (**1**) and also for the other dimer of compound (**2**) (–19.9 kcal/mol) represented in Fig. 7b. These results show that the binding energies for the interaction of either a carboxylic or a carboxylate group with neutral or protonated adenine through its Hoogsteen face are similar.

For compound (**3**), we have analysed the self-assembled dimer shown in Fig. 8 and the interaction energy is ΔE_5 = –12.1 kcal/mol, in excellent agreement with that computed using the QTAIM (–12.8 kcal/mol). It is worthy to comment that the binding energy of this dimer is smaller compared to the equivalent dimer computed for neutral compound (**1**) (see Fig. 6c) in line with the longer H-bonds, likely provoked by the protonation of the adenine rings.

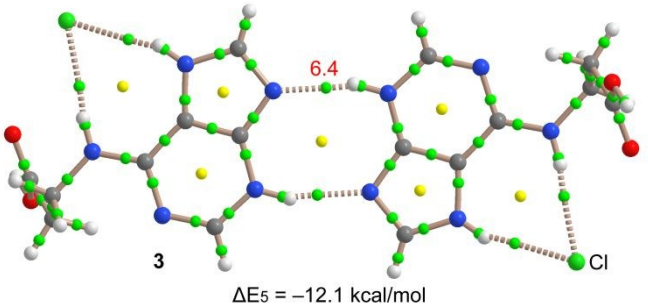

Fig. 8 AIM distribution of bond and ring critical points (green and yellow spheres, respectively) and bond paths obtained for one self-assembled dimers of compound (**3**). The interaction energy is indicated. The dissociation energy of the H-bond using the G(r) values at the bond CP are indicated in red (kcal/mol).

In compound (**4**), we have analysed two H-bonded self–assembled dimers (see Fig. 9a,b) and the anion–π interaction (see Fig. 9c). The interaction energy of the double N(7)–H···N(3) self-assembled dimer (see Fig. 9a) is ΔE_6 = –9.6 kcal/mol, also in excellent agreement with that computed using the QTAIM method (–9.2 kcal/mol). This suggests that the QTAIM is an excellent tool to predict the individual H-bonding energies in adenine derivatives. The other self-assembled dimer where two symmetrically equivalent carboxylic···adenine interactions through the Hoogsteen face are established is significantly more favoured (ΔE_7 = –22.4 kcal/mol) due to the formation of four H-bonds. In general, the H-bond energies are smaller for the hydrochloride salts than for the neutral adenines. Finally, the QTAIM analysis of the anion–π complex (see Fig. 9c) shows a bond CP and bond path connecting the Cl anion to the N(1) atom of the adenine ring, thus confirming the existence of the interaction.[32]

Moreover, the interaction energy is significant (ΔE_8 = –17.2 kcal/mol) thus suggesting a relevant role in the crystal packing of (**4**). The distribution of bond CPs also shows a bond path that connects the anion to one H-atom of the alkyl chain. However, the contribution of this C–H···Cl interaction is very week (–0.8 kcal/mol).

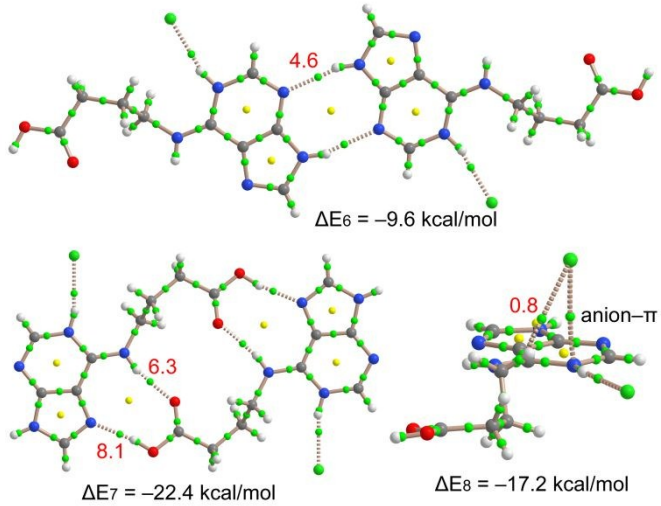

Fig. 9 (a,b) AIM distribution of bond and ring critical points (green and yellow spheres, respectively) and bond paths obtained for two self-assembled dimers of compound (**4**). (c) AIM distribution of bond and ring critical points (green and yellow spheres, respectively) and bond paths obtained for the anion–π complex of (**4**). The interaction energies are indicated. The dissociation energy of the H-bond using the G(r) values at the bond CP are indicated in red (kcal/mol).

4. Concluding remarks

We have synthesized and X-ray characterized several derivatives of N^6-akylcarboxy functionalized adenine and their corresponding hydrochloride salts. We have studied and rationalized the changes in the dimerization patterns of adeninium cation because of the competition between homodimerization and cross-dimerization between the carboxylic group and the Hoogsteen face of adenine/adeninium cation. DFT studies and QTAIM analysis revealed that the feasibility for self-dimerization through the carboxylic group is favoured with respect to homodimerization. The energetic study and evaluation of individual contributions is useful in terms of mimicking adenine-aspartic/glutamic acid interactions and for the parametrisation of force fields.

Conflicts of interest

There are no conflicts to declare.

Acknowledgements

AF thanks the MINECO/AEI from Spain for a "Juan de la Cierva" contract. We thank the MINECO/AEI from Spain for financial support (project numbers CTQ2017-85821-R, ENE2015-63969-C3-3-R, BIO2016-78057-R and SEV2015-0496,

FEDER funds and CTQ2017-90802-REDT). Also thanks the Direcció General de Recerca i Innovació del Govern Balear (AAEE039/2017) for funding. We thank the CTI (UIB) and CACTI (UVigo) for free allocation of computer time and single crystal X-ray diffraction facilities, respectively.

References

‡These compounds did not show cytotoxic activity against HeLa cells. The experiment was done using the highly sensitive PrestoBlue reagent to assess cell viability and cytotoxicity, see *J. Pharmcol. Toxicol. Methods*, 2015, **71**, 1-7

1 H. Rosemeyer, *Chem*. *Biodiversity*, 2004, **1**, 361–401.
2 (a) M. Legraverend, Tetrahedron, 2008, 64, 8585–8603; (b) M. Legraverend and D. S. Grierson, *Bioorg. Med. Chem*., 2006, **14**, 3987–4006.
3 G. Shaw, in Comprehensive Heterocyclic Chemistry, Vol. 5 (Eds.: A. Katritzky, C. Rees), Pergamon, Oxford, 1984..
4 H. Kosaku, K. Kazunori, N. Itaru, K. Hiroshi, S. Hironao, I. Yoshiaki, T. Haruo, T. Masanori, O. Haruhisa, O. Tetsuhiro, I. Shinji, K. Ayumu and K. Hajime, *J. Med. Chem*., 2002, **45**, 5419–5422.
5 (a) A. Kurimoto, T. Ogino, S. Ichii, Y. Isobe, M. Tobe, H. Ogita, H. Takaku, H. Sajiki, K. Hirota and H. Kawakami, *Bioorg. Med. Chem*. 2003, **11**, 5501–5508; (b) A. Kurimoto, T. Ogino, S. Ichii, Y. Isobe, M. Tobe, H. Ogita, H. Takaku, H. Sajiki, K. Hirota and H. Kawakami, *Bioorg. Med. Chem*., 2004, **12**, 1091–1099.
6 Y.-T. Chang, S. M. Wignall, G. R. Rosania, N. S. Gray, S. R. Hanson, A. I. Su, J. Merlie Jr., H.-S. Moon, S. B. Sangankar, O. Perez, R. Heald and P. G. Schultz, *J. Med. Chem*. 2001, **44**, 4497–4500.
7 (a) B. Dymock, X. Barril, M. Beswick, A. Collier, N. Davies, M. Drysdale, A. Fink, C. Fromont, R. E. Hubbard and A. Massey, *Bioorg. Med. Chem. Lett*., 2004, **14**, 325–328; (b) A. Maloney and P. Workman, *Expert Opin. Biol. Ther*., 2002, **2**, 3–24; (c) G. Chiosis, Curr. Top. Med. Chem., 2006, **6**, 1183–1191; (d) T. Taldone and G. Chiosis, *Curr. Top. Med. Chem*., 2009, **9**, 1436–1446.
8 J. Robichaud, R. Oballa, P. Prasit, J.-P. Falgueyret, M. D. Percival, G. Wesolowski, S. B. Rodan, D. Kimmel, C. Johnson, C. Bryant, S. Venkatraman, E. Setti, R. Mendonca and J. T. Palmer, *J. Med. Chem*., 2003, **46**, 3709–3727.
9 P. Figueiredo, M. Costa, O. Pontes, F. Baltazar and F. Proença, *Eur. J. Org. Chem*., 2018, 3943–3956
10 E. Altmann, S. W. Cowan-Jacob and M. Missbach, *J. Med. Chem.*, 2004, **47**, 5833–5836.
11 (a) P. Raboisson, C. Lugnier, C. E. Muller, J.-M. Reimund, D. Schultz, G. Pinna, A. Le Bec, H. Basaran, L. Desaubry, F. Gaudiot, M. Selouma and J.-J. Bourguignon, *Eur. J. Med. Chem*., 2003, **38**, 199–214; (b) J. W. F. Whitehead, G. P. Lee, P. Gharagozloo, P. Hofer, A. Gehrig, P. Wintergerst, D. Smyth, W. McCoull, M. Hachicha, A. Patel and D. J. Kyle, *J. Med. Chem*., 2005, **48**, 1237–1243; (c) X. Qiu, Y. Huang, D. Wu, F. Mao, J. Zhu, W. Yan, B. H. Luo and J. Li, *Bioorg. Med. Chem*., 2018, **26**, 119–133.
12 (a) S. A. Laufer, D. M. Domeyer, T. R. Scior, W. Albrecht and D. R. Hauser, *J. Med. Chem*. 2005, **48**, 710–722
13 (a) K. A. Jacobson and G. Zhan-Guo, *Nat. Rev. Drug Discovery*, 2006, **5**, 247–264; (b) G. Haskó, J. Linden and P. Pacher, *Nat. Rev. Drug Discovery*, 2008, 7,759–770; (c) L. Antonioli, C. Blandizzi, P. Pacher and G. Haskó, *Nat. Rev. Cancer*, 2013, **13**, 842–857; (d) J.-F. Chen, H. K. Eltzschig and B. B. Fredholm, *Nat. Rev. Drug Discovery*, 2013, 12, 265–286; (e) J. L. Adams, J. Smothers, A. Hoos, *Nat. Rev. Drug Discovery*, 2015, **14**, 603–622; (f) D. Allard, M. Turcotte and J. Stagg, *Immunol. Cell Biol*., 2017, **95**, 333–339; (g) C. Cekic and J. Linden, *Nat. Rev. Immunology*. 2016, **16**, 177–192; (h) D. Vijayan, A. Young and M. J. Smyth, *Nat. Rev. Cancer*, 2017, **17**, 709–724.
14 (a) M. Perreira, J.-K. Jiang, A. M. Klutz, Z.-G. Gao, A. Shainberg, C. Lu, C. J. Thomas and K. A. Jacobson, *J. Med. Chem*., 2005, **48**, 4910–4918; (b) P. G. Baraldi, D. Preti, M. A. Tabrizi, F. Fruttarolo, R. Romagnoli, N. A. Zaid, A. R. Moorman, S. Merighi, K. Varani and P. A. Borea, *J. Med. Chem*., 2005, **48**, 4697–4701; (c) K. Xu, E. Bastia and M. Schwarzschild, *Pharmacol. Ther*. 2005, **105**, 267–310; (d) W. B. Parker, *Chem. Rev*., 2009, **109**, 2880–2893; (e) S. Basu, D. A. Barawkar, V. Ramdas, Y. Waman, M. Patel, A. Panmand, S. Kumar, S. Thorat, R. Bonagiri, D. Jadhav, P. Mukhopadhyay, V. Prasad, B. S. Reddy, A. Goswami, S. Chaturvedi, S. Menon, A. Quraishi, I. Ghosh, S. Dusange, S. Paliwal, A. Kulkarni, V. Karande, R. Thakre, G. Bedse, S. Rouduri, J. Gundu, V. P. Palle, A. Chugh and K. A. Mookhtiar, *Eur. J. Med. Chem*. 2017, 127, 986–996.
15 (a) A. García-Raso, C. Cabot, J. J. Fiol, L. Spichal, J. Nisler , A. Tasada, J. M. Luna, F. M. Albertí and I. V. Sibole, *J. Plant Physiol*., 2009, **14**, 1529 -1536. (b) D. W. Mok and M. C. Mok, *Annu. Rev. Plant Physiol. Plant Mol. Biol*., 2001, **89**, 89 -118
16 (a) K. Dolezal, I. Popa, V. Krystof, L. Spichal, M. Fojtikova, J. Holub, R. Lenobel, T. Schmulling and M. Strnad, *Bioorg. Med. Chem.,* 2006, **14**, 875-884. (b) K. Vemeulen, M. Strnad, L. Havlicek, H. Van Onckelen, M. Lenjou, G. Nijs, D. R. Van Bockstaele and Z. N. Berneman, *Exp. Hematol*., 2002, **30**, 1107 -1114. (c) L. Szucova, Z. Travnicek, M. Zatloukal and I. Popa, *Bioorg. Med. Chem*., 2006, **14**, 479-491; (d) M. Strnad *Physiol. Plant*., 1997, **101**, 674-688; (e) T. Umemoto, J. Wengel and A. S. Madsen, *Org. Biomol. Chem*., 2009, 7, 1793 -1797
17 (a) P. Narayanan, H. M. Berman and R. Rousseau, *J. Am. Chem. Soc*., 1976, **98**, 8472-8475; (b) A. F. Mishnev, J. Bleidelis, I. N. Goncharova and N. P. Ramzaeva, *Latv. PSR Zinat. Akad. Vestis, Khim. Ser*., 1982, 321-324; (c) P. V. Krasnov, A. Y. Vigorov, V. V. Musiyak, I. A. Nizova, D. A. Gruzdev, T. V. Matveeva, G. L. Levit, M. A. Kravchenko, S. N. Skornyakov, O. B. Bekker, V. N. Danilenko and V. N. Charushin, *Bioorg. Med. Chem. Lett*., 2016, **26**, 2645-2648; (d) D. A. Gruzdev, E. N. Chulakov, G. L. Levit, M. A. Kravchenko, V. P. Krasnov and V. N. Charushin, *Mendeleev Commun*., 2017, **27**, 547-549
18 A. García-Raso, A. Terrón, A. Bauzá, A. Frontera, J. J. Molina, E. M. Vázquez-López and J. J. Fiol, *New J. Chem*., 2018, **42**, 14742-14750.
19 (a) J.M. Lehn, *Supramolecular Chemistry*, VCH, Weinheim, Germany, 1995; (b) J. W. Steed and J. L. Atwood, *Supramolecular Chemistry*, Wiley, Chichester, U.K., 2000.
20 A. Terrón, J. J. Fiol, A. García-Raso, M. Barceló-Oliver, V. Moreno, *Coord. Chem. Rev*., 2007, **251**, 1973-1986.
21 M. Barceló-Oliver, A. Tasada, J. J. Fiol, A. García-Raso, A. Terrón and E. Molins, *Polyhedron* 2006, **25**, 71-80.
22 (a) Bruker ASX Inc., APEX3, SAINT and SADABS. Madison, Wisconsin, USA (2014). (b) G.M. Sheldrick *Acta Crystallogr. C*, 2015, 71, 3-8.
23 Gaussian 09, Revision C.01, M. J. Frisch, G. W. Trucks, H. B. Schlegel, G. E. Scuseria, M. A. Robb, J. R. Cheeseman, G. Scalmani, V. Barone, B. Mennucci, G. A. Petersson, H. Nakatsuji, M. Caricato, X. Li, H. P. Hratchian, A. F. Izmaylov, J. Bloino, G. Zheng, J. L. Sonnenberg, M. Hada, M. Ehara, K. Toyota, R. Fukuda, J. Hasegawa, M. Ishida, T. Nakajima, Y. Honda, O. Kitao, H. Nakai, T. Vreven, J. A. Montgomery, Jr., J. E. Peralta, F. Ogliaro, M. Bearpark, J. J. Heyd, E. Brothers, K. N. Kudin, V. N. Staroverov, R. Kobayashi, J. Normand, K. Raghavachari, A. Rendell, J. C. Burant, S. S. Iyengar, J. Tomasi, M. Cossi, N. Rega, J. M. Millam, M. Klene, J. E. Knox,

View Article Online
DOI: 10.1039/C9NJ02279A

J. B. Cross, V. Bakken, C. Adamo, J. Jaramillo, R. Gomperts, R. E. Stratmann, O. Yazyev, A. J. Austin, R. Cammi, C. Pomelli, J. W. Ochterski, R. L. Martin, K. Morokuma, V. G. Zakrzewski, G. A. Voth, P. Salvador, J. J. Dannenberg, S. Dapprich, A. D. Daniels, Ö. Farkas, J. B. Foresman, J. V. Ortiz, J. Cioslowski, and D. J. Fox, Gaussian, Inc., Wallingford CT, 2009.

24 Y. Zhao and D. G. Truhlar, *Theor. Chem. Acc.*, 2008, **120**, 215-241.

25 (a) G. Mahmoudi, S. K. Seth, A. Bauza, F. I. Zubkov, A. V. Gurbanov, J. White, V. Stilinovic, T. Doert and A. Frontera, *CrystEngComm*, 2018, **20**, 2812-2821; (b) C. Martínez-Benito, A. Bauzá, A. B. Lago, C. Ruiz-Pérez, C. A. Jiménez, M. E. Torres, A. Frontera and J. Pasán, *Cryst. Growth Des.*, 2018, **18**, 2636-2644; (c) S. Roy, M. G. B. Drew, A. Bauzá, A. Frontera and S. Chattopadhyay, *CrystEngComm*, 2018, **20**, 1679-1689; (d) S. Ghosh, S. Biswas, A. Bauzá, M. Barceló-Oliver, A. Frontera and A. Ghosh, *Inorg. Chem.*, 2013, **52**, 7508-7523.

26 S. F. Boys and F. Bernardi, *Mol. Phys.*, 1970, **19**, 553-566.

27 T. A.Keith, AIMAll (Version 13.05.06), TK Gristmill Software, Overland Park, KS, 2013.

28 (a) J. S. Nirmalram, D. Tamilselvi and P. T. Muthiah, *J. Chem. Crystallogr.*, 2011, **41**, 864–867; (b) S. J. Jennifer, P. Thomas Muthiah and D. Tamilselvi, *Chem. Cent. J.*, 2014, **8**, 58; (c) D. Tamilselvi and P. T. Muthiah, *Acta Cryst.*, 2011, **C67**, o192–o194.

29 C. McHugh and A. Erxleben, *Cryst. Growth Des.*, 2011, **11**, 5096–5104.

30 (a) M. Takimoto, A. Takenaka and Y. Sasada, *Bull. Chem. Soc. Jpn.*, 1981, **54**, 1635–1639. (b) J. Kumar, S. Awasthi, and S. Verma, *Cryst. Growth Des.*, 2010, **10**, 3555-3561.

31 M. V. Vener, A. N. Egorova, A. V. Churakov and V. G. Tsirelson, *J. Comput. Chem*. 2012, **33**, 2303–2309

32 R. F. W. Bader, *J. Phys. Chem. A*, 1998, **102**, 7314–7323

View Article Online
DOI: 10.1039/C9NJ02279A

H-bonding networks and anion–π interactions in crystal structures of N^6-modified-aminoacid adenine analogs are investigated using X-ray crystallography and DFT calculations.